JOURNAL OF AIRCRAFT
Vol. 30, No. 3, May–June 1993

Multiblock Navier-Stokes Solutions About the F/A-18 Wing-LEX-Fuselage Configuration

Farhad Ghaffari,* James M. Luckring,† and James L. Thomas‡
NASA Langley Research Center, Hampton, Virginia 23665
Brent L. Bates§
Vigyan, Inc., Hampton, Virginia 23666
and
Robert T. Biedron§
Analytical Services and Materials, Inc., Hampton, Virginia 23666

Three-dimensional thin-layer Navier-Stokes computations are presented for the F/A-18 configuration. The modeled configuration includes an accurate surface representation of the fuselage, leading-edge extension (LEX), and wing, both with and without leading-edge flap deflection. A multiblock structured grid strategy is employed to decompose the computational flowfield domain around the subject configuration. Steady-state solutions are obtained from an algorithm that solves the compressible Navier-Stokes equations with an upwind-biased, flux-difference splitting approach. The results presented are based on a fully turbulent flow assumption, simulating the high Reynolds number flow conditions that correspond to a recent F/A-18 flight experiment. Good agreements between the computations and the flight test results are obtained for both surface flow patterns as well as surface pressure distributions. Furthermore, a correlation between the computed LEX vortex-core and the flight test results, observed by way of smoke visualization, is also presented.

Nomenclature

C_D = drag coefficient, drag/$q_\infty S_{\text{ref}}$
C_L = lift coefficient, lift/$q_\infty S_{\text{ref}}$
C_p = pressure coefficient, $(p - p_\infty)/q_\infty$
c_p = specific heat at constant pressure, ft-lb/slug°R
c_v = specific heat at constant volume, ft-lb/slug°R
$\bar{c}$ = wing mean aerodynamic chord, 11.52 ft
E_0 = total energy per unit volume
$\hat{F}, \hat{G}, \hat{H}$ = flux vectors
J = Jacobian of the coordinate transformation
k = conductivity, $c_p\mu/Pr$, lb/s°R
M_∞ = freestream Mach number
Pr = Prandtl number
$\hat{Q}$ = state vector, $J^{-1}(\rho, \rho u, \rho v, \rho w, E_0)^T$
q_∞ = freestream dynamic pressure, lb/ft^2
$R_{\bar{c}}$ = Reynolds number based on $\bar{c}$
S_{ref} = area of reference wing planform, 400 ft^2
u, v, w = body-axis Cartesian velocity components, ft/s
v^* = wall-friction velocity, $\sqrt{\tau_w/\rho}$, ft/s
y^+ = inner-law variable, yv^*/ν
y/s = fraction of LEX exposed semispan
α = angle of attack, deg
γ = ratio of specific heats, c_p/c_v
δ_f = flap deflection angle, deg
θ = azimuthal angle, deg
μ = viscosity, lb-s/ft^2
ν = kinematic viscosity, μ/ρ, ft^2/s
ξ, η, ζ = body-fitted coordinates
ρ = density, slug/ft^3
τ_w = wall shear stress, lb/ft^2

Presented as Paper 91-3291 at the AIAA 9th Applied Aerodynamics Conference, Baltimore, MD, Sept. 23–25, 1991; received Dec. 9, 1991; revision received March 19, 1992; accepted for publication March 19, 1992.

*Research Engineer, Transonic Aerodynamics Branch, Applied Aerodynamics Division. Senior Member AIAA.
†Head of Transonic Aerodynamics Branch, Applied Aerodynamics Division. Associate Fellow AIAA.
‡Head of Computational Aerodynamics Branch, Fluid Mechanics Division. Associate Fellow AIAA.
§Research Engineer. Member AIAA.

Introduction

IN recent years, computational fluid dynamics (CFD) has reached the level of maturity where it can be applied to investigate complex flow structures over an aircraft configuration. One such flow structure is the inevitable vortical flow that occurs over highly maneuverable fighter-type aircraft at high angles of attack. In general, the presence of such vortical flow over an airborne vehicle can be advantageous, so long as it remains organized and stable, giving rise to what is known as "vortex lift" for enhanced performance. However, with increasing angle of attack, such a coherent vortex system is susceptible to instabilities such as breakdown or flow asymmetry causing undesirable pitching, yawing, and/or rolling moments. As a result, the flight handling quality and controllability of these aircraft are severely effected by such flow phenomenon; they often limit the ability of the vehicle to maneuver with high agility. It is critically important to understand this flow phenomenon and to develop technology that can accurately predict the formation of such flow over a wide range of flight conditions. CFD has been widely recognized as a viable aerodynamic tool that can be utilized to address such issues.

Presently, there is a concerted effort among the aerodynamic research community that is specifically designed to provide an understanding of and means to explore high angle-of-attack aerodynamics. This research activity is providing extensive flow analyses, supported by a unique set of data gathered from a wide range of resources such as flight tests, wind-tunnel experiments, and CFD simulations. An F/A-18 aircraft, designated as the high alpha research vehicle (HARV), was chosen for this activity primarily due to its high angle-of-attack capability and has been highly instrumented for pressure measurements as well as for in-flight flow visualization,

both on- and off-surface. The HARV flight experiments are being conducted by NASA at the Dryden Flight Research Facility.

The CFD analysis of high angle-of-attack flow has been very successful in the past few years through the application of advanced numerical codes to simulate the flow about the isolated F/A-18 forebody including the leading-edge extension (LEX).[1-3] This progress is mainly attributed to the recent advances made in the numerical algorithms and volume grid generation techniques, as well as the increase in computer speed and capacity. As a result, a plan was initiated to include more of the F/A-18 geometrical components such as the wing, aft portion of the fuselage, empennage, etc. to the computations. Two different approaches were taken for adding more geometrical features of the aircraft to the earlier isolated forebody-LEX computations. Although both approaches are based on multiblock structured grids, one uses an overset grid or Chimera[4,5] approach which has been reported in Refs. 6–8; the other approach, the subject of this article, is based on a newly developed generalized surface patching algorithm[9] for nonoverlapping blocked grids.

The purpose of the present investigation is to compute the flow about an accurate and fairly complete representation of the F/A-18 configuration using state-of-the-art Navier-Stokes methodology. This study is an extension to the previously reported computations, about the isolated forebody-LEX configuration,[1] by including the remainder of the fuselage as well as the wing geometry with two different flap settings. Consistent with the previous computations, an accurate surface definition for all geometrical components is developed for meaningful CFD analysis. Subsequently, a unique multiblock flowfield grid strategy is adopted with various topologies appropriate for resolving all relevant local geometrical features as well as the expected flow phenomena. The computations are performed at flow conditions ($M_\infty = 0.34$, $R_c = 13.5 \times 10^6$, and $\alpha = 19$ deg) that correspond to a recent HARV flight-test. Furthermore, at these conditions the flow is expected to be fully turbulent, with the exception of a small region near the nose apex where the flow would be transitional. Therefore, the present study will only focus on fully turbulent computations.

Computational Methodology

The governing equations as well as the computational method for the present investigation have been published many times in the open literature[1,2,10-12] as they have evolved. The flow is presumed to be governed by the unsteady Reynolds-averaged Navier-Stokes equations which are written in a body-fitted coordinate system. They are written in a usual conservation-law form as

$$\hat{Q}_{,t} + (\hat{F} - \hat{F}_v)_{,\xi} + (\hat{G} - \hat{G}_v)_{,\eta} + (\hat{H} - \hat{H}_v)_{,\zeta} = 0$$

Here the subscripts with a comma denote partial differentiation, the subscript v identifies the viscous terms, and the superscript $\hat{}$ indicates scaling with respect to the Jacobian of the coordinate transformation. Details for these terms are included in Ref. 13. In addition to the ideal gas assumption in the present study, the thin layer approximation to the governing equations is invoked (i.e., $\hat{F}_v = \hat{G}_v = 0$) thus accounting for viscous flux terms only in the ζ direction (normal to the body).

Turbulence effects are accounted for through the notion of an eddy viscosity and eddy conductivity

$$\mu = \mu_l + \mu_t = \mu_l(1 + \mu_t/\mu_l)$$

$$k = k_l + k_t = k_l(1 + k_t/k_l) = (c_p\mu_l/Pr_l)[1 + (\mu_t Pr_l/\mu_l Pr_t)]$$

where the subscripts l and t denote laminar and turbulent, respectively. The algebraic turbulence model developed by Baldwin and Lomax[14] is used to evaluate the required turbulence quantities. For separated vortical flow regions, the notions of Degani and Schiff[15] are drawn upon to ensure that the proper turbulence length scales are used.

Discretization of the governing equations results in a consistent approximation to the conservation laws in integral form

$$\frac{\partial}{\partial t}\int\int\int \hat{Q}\, dV + \int\int \hat{f}\cdot\hat{n}\, dS = 0$$

where the time rate of change of the state vector $\hat{Q}$ within a cell is balanced by the net flux $\hat{f}$ across the cell surface. The convective and pressure flux quantities are represented using the upwind biased, flux-difference-splitting approach of Roe.[16] The monotone upstream-centered scheme for conservation laws (MUSCL) approach of van Leer[17] is used to determine state-variable interpolations at the cell interfaces. Salient aspects of this formulation are included in Appendix 2 of Ref. 13 and additional details have been given by Vatsa et al.[12] Futhermore, a detailed discussion on the algorithm developments for interpolating the mass, momentum, and energy across the various planar and nonplanar interfaces that separate the grid blocks is presented by Biedron and Thomas.[9]

Surface Definition and Grid

The surface patch definition of the complete F/A-18 aircraft was obtained from a detailed computer aided design (CAD) description in a format known as initial graphics exchange specification (IGES).[18] This data was then used to extract a high-density surface grid definition in the form of cross sections. This CFD data base grid consisted of approximately 30,000 grid points on the fuselage defined at 60 cross sections and 16,000 points on the wing defined at 20 streamwise cuts. Although not used in the present computations, a high-fidelity surface definition for both horizontal as well as vertical tails was included in this data base for future application.

This data base was subsequently used to generate a coarser and more suitable surface grid for Navier-Stokes computation by employing an Overhauser[19] function for the interpolation; this function has been shown to alleviate the oscillatory behavior inherent in other widely used functions, such as splines, in the region where grid point distributions are not uniform. The final computational surface grid was composed of approximately 18,000 points. The geometrical simplifications made to the configuration included fairing over the inlet, splitter plate, diverter, and the LEX slot. Figure 1a shows a body cross section at $x = 401.0$ illustrating the simplifications made to the lower part of the splitter plate. Similarly, Fig. 1b shows a body cross section at $x = 441.0$ illustrating the closing of the LEX slot, as well as the fairing over the cavity

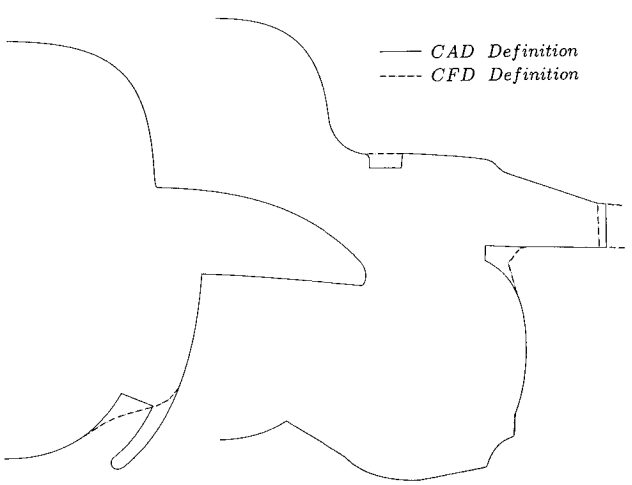

a) $x = 401$ in. b) $x = 441$ in.

Fig. 1 Typical CAD/CFD cross-sectional grid.

region between the inlet and the LEX lower surface. The latter simplification is made to a limited region to ease the grid generation in that area. Furthermore, the wing geometry is modeled with two different leading-edge flap representations, the "undeflected" and "blended-flap"; the latter will be discussed in the next paragraph. Two orthographic views of the final F/A-18 CFD surface grid definition with undeflected flap are shown in Fig. 2 to illustrate the overall grid resolution.

The F/A-18 wing leading-edge flap deflection angle varies as a function of angle of attack and Mach number. The flap deflection angle for the present freestream flow-conditions of interest ($M_\infty = 0.34$, $R_\varepsilon = 13.5 \times 10^6$, and $\alpha = 19$ deg) corresponds to $\delta_f \approx 25$ deg. An approximate geometrical surface representation for the wing leading-edge flap deflection, designated as blended flap, is considered in the present computation. The underlying principal behind the deflected-flap geometry modification was to preserve the wing-body (with undeflected flap) intersection, therefore allowing for the same overall blocking strategy to be used for both undeflected as well as blended flap configuration. This modification is implemented over the inboard 15% semispan of the flap by smoothly blending from the deflected flap geometry to the undeflected flap wing-body intersection. With this approach, the maximum spanwise blending occurred at the leading edge and gradually diminished to zero at the flap hinge line. The neighboring surface grid definition outside the blended region is used to ensure smooth surface-curvature transition across the boundaries. A nosedown front view of the F/A-18 CFD surface grid definition with both the blended flap (starboard) and undeflected-flap (port) is shown in Fig. 3. This blending modification of the deflected flap also simplified the complex modeling of the gap region (closed in present computations) which would otherwise occur between the inboard face of the deflected flap and the fuselage.

The F/A-18 configuration can be categorized longitudinally into two distinct classes of aerodynamic shape in terms of aspect ratio, with a dividing line at the wing-LEX juncture.

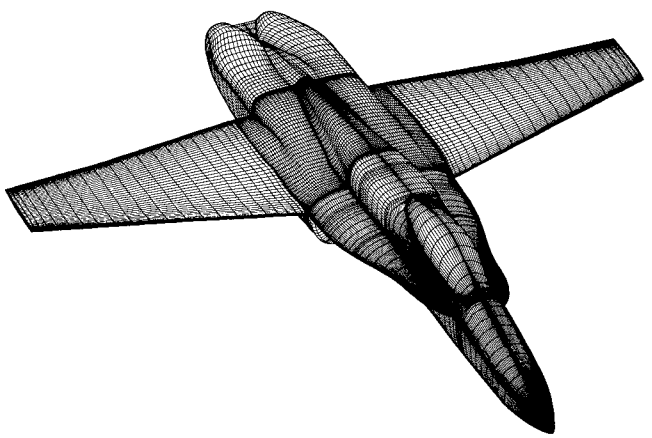

a) Oblique top view

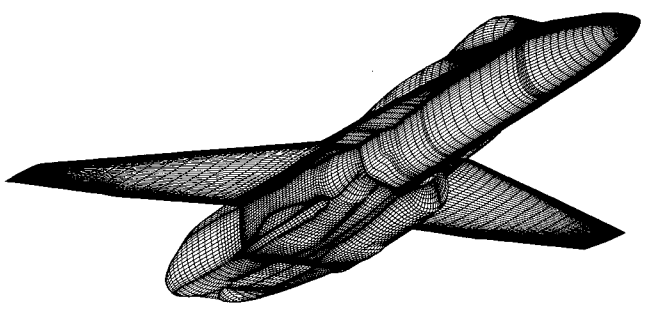

b) Oblique bottom view

Fig. 2 F/A-18 CFD surface grid representation.

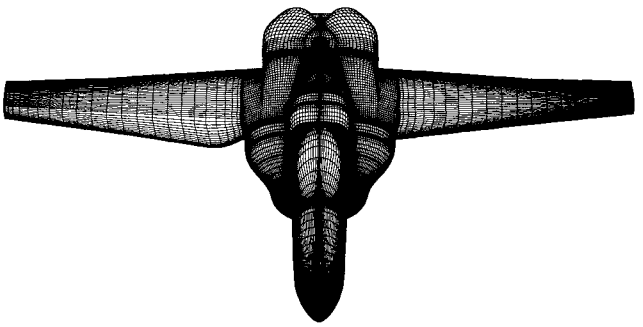

Fig. 3 F/A-18 CFD surface grid with undeflected (port) and blended (starboard) flap.

The front part of the vehicle, which includes the forebody and the LEX, can be classified as a slender body-type configuration, whereas the aft part is a high-aspect ratio-type configuration. From a CFD analysis point of view, these two classes of configuration require different grid topologies in order to efficiently resolve the corresponding flowfield. An H-O grid topology is usually chosen for slender type configuration, whereas a C-O grid is typically used for high-aspect ratio wings. It is inappropriate to exchange the above topologies with one another for a given class of configuration.

The challenge of defining a grid strategy for the entire configuration was in fact to find a way to link the various necessary grid topologies appropriate for each part while maintaining grid quality. To illustrate the selected global grid strategy, an isometric far-field view of the configuration surface shading is shown in Fig. 4, along with the field grids in the plane of symmetry as well as the configuration maximum half-breadth plane. For clarity, the grid density shown in the figure has been reduced in both longitudinal and radial directions. The flowfield domain, consisting of about 1.24 million grid points, is broken into five regions, each comprised of one or more topologically similar blocks. In Fig. 4, each region is highlighted with a different color, and block boundaries are denoted by thick solid lines. Region one (yellow) consists of a single block that represents the forebody with a C-O topology and 75,075 grid points. Region two (red) consists of four H-O blocks that are used to model the LEX as well as the canopy with 278,655 points. Region three (cyan) approximately covers the aft part of the fuselage and comprises 12 blocks, each having an H-H topology, with a total of 510,315 grid points. In this region, the blocks are evenly divided with the grids for the upper six blocks generated from the fuselage upper surface definition, and similarly the grids for the lower six blocks are generated from their respective fuselage lower surface definition. Region four (magenta) consists of two blocks both having an H-O topology with total of 156,780 grid points. Region five (green) is a single block with a C-O topology generated about the wing surface grid and includes part of its trailing wake with a total of 220,350 points. As evident, region three contains the highest concentration of grid points in the flowfield. This is primarily due to the enforcement of the one-to-one surface grid matching between the wing and fuselage, so that the longitudinal stations on the fuselage correspond to the chordwise surface grid definition on the wing.

A side view of the flowfield grid for selected surfaces is shown in Fig. 5 to illustrate the various regions (discussed above) from a different perspective. The figure depicts the overall far-field boundary along with the wing region carved out of the field domain and shown in the lower right corner. Again, the boundaries between the various regions and their interior blocks are highlighted by colors and thick solid lines, respectively. Three factors contributed to the selection of the grid topology for each region. These were the local geometrical consideration, the proper resolution of the expected flow structure, and finally the appropriate grid connectivity between regions. The selected topologies provided good res-

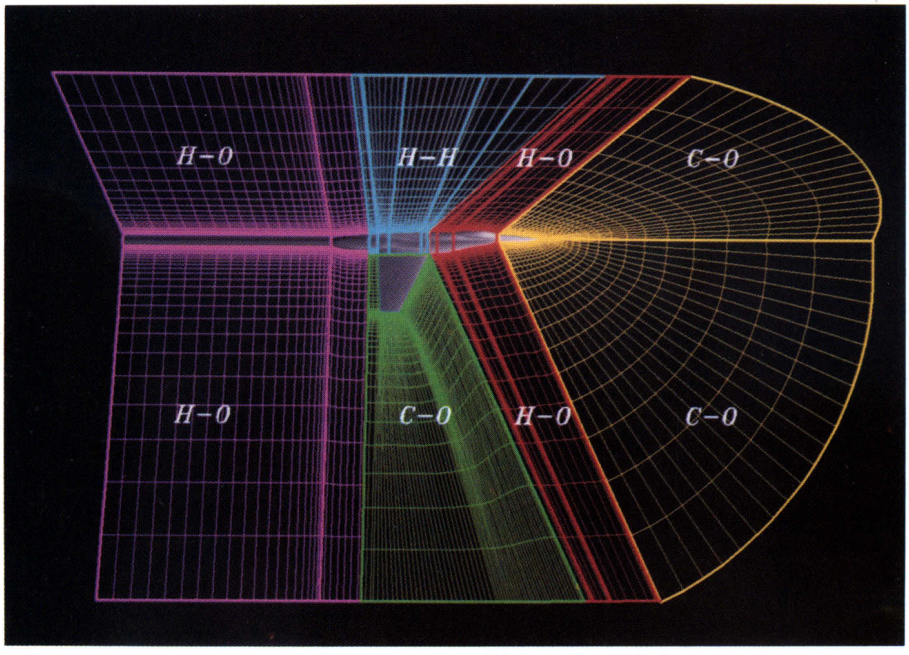

Fig. 4 F/A-18 flowfield blocking strategy–far-field view.

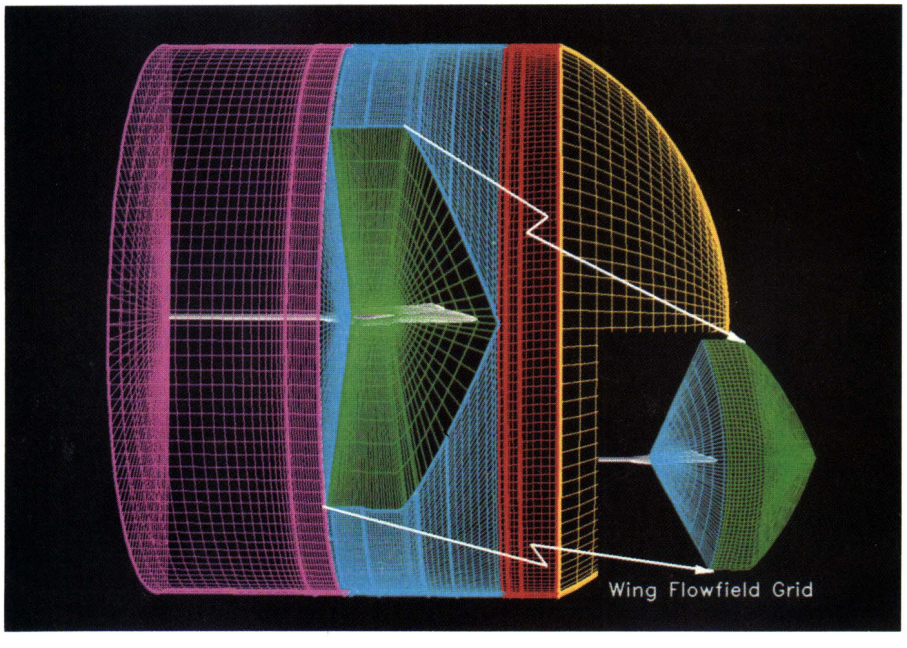

Fig. 5 F/A-18 flowfield blocking strategy–far-field sideview.

olution of all edge flows (i.e., LEX and wing leading edges, wing side edge, etc.) as well as the juncture flows (i.e., LEX-body, wing-body, canopy-body, etc.)

The flowfield grid is generated using established transfinite interpolation techniques[1,20] with sufficient normal clustering near the surface to adequately resolve the laminar sublayer for the turbulent boundary-layer flow at the subject flight freestream conditions ($M_\infty = 0.34$, $R_{\bar{c}} = 13.5 \times 10^6$, and $\alpha = 19$ deg). This grid produced an average normal cell size next to the wall of approximately $7.2 \times 10^{-6}\ \bar{c}$ which corresponds to $y^+ \approx 3$ for the turbulent computations; a laminar sublayer generally extends out to $y^+ \approx 8.5$. The radial far-field boundary and the downstream grid extension is about $7.6 \times \bar{c}$, and $4.7 \times \bar{c}$, respectively.

Results and Discussion

All computations are performed on the numerical aerodynamic simulation (NAS) Cray-2, located at NASA-Ames. On this machine, the algorithm requires approximately 20 μs/grid point/cycle and about 100-million words of memory. Converged results for the undeflected flap case are obtained in nominally 3000 cycles requiring about 20 h of computer time. This number of cycles was sufficient to reduce the residuals by a little more than two orders of magnitude and to reduce oscillations in C_L and C_D to a negligible level. Subsequently, the solution was restarted for the blended flap case and required about 3500 cycles for the residuals to drop approximately 2.5 orders of magnitude and consumed about 24 h of computer time. The computations are performed without the use of mesh sequencing or multigrid iteration.

Computational Flow Features

The total pressure contours in various crossflow planes along with the LEX vortex core streamlines as well as a few off-surface wing flowfield streamlines are shown in Fig. 6a. The results shown are obtained with the turbulent flow assumption at flow conditions of $M_\infty = 0.34$, $R_{\bar{c}} = 13.5 \times 10^6$, and $\alpha = 19$ deg for the undeflected wing leading-edge flap case. The magnitudes associated with contour quantities are displayed using a color bar with white indicating the maximum

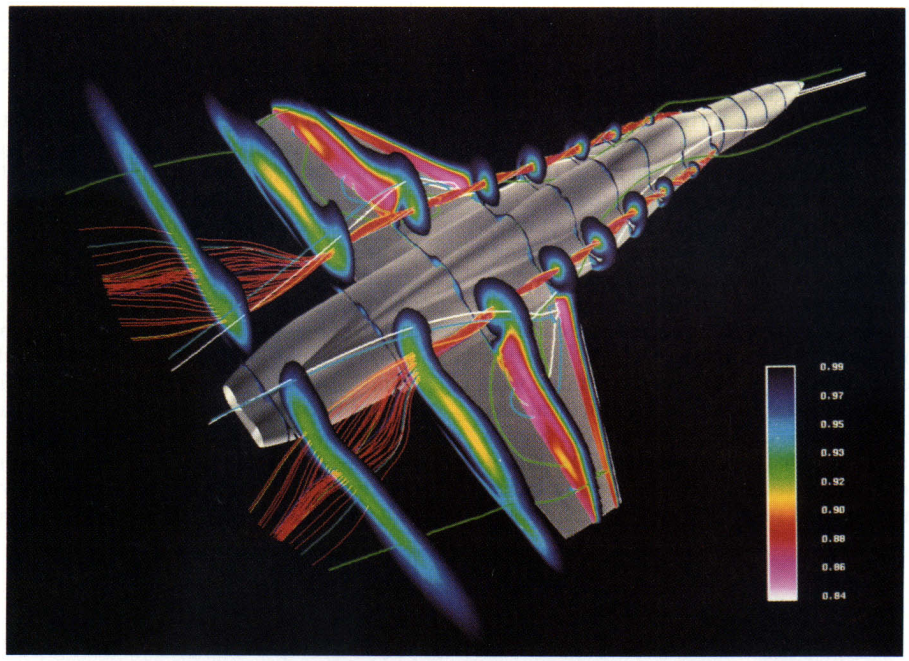

a) $\delta_f = 0$ deg

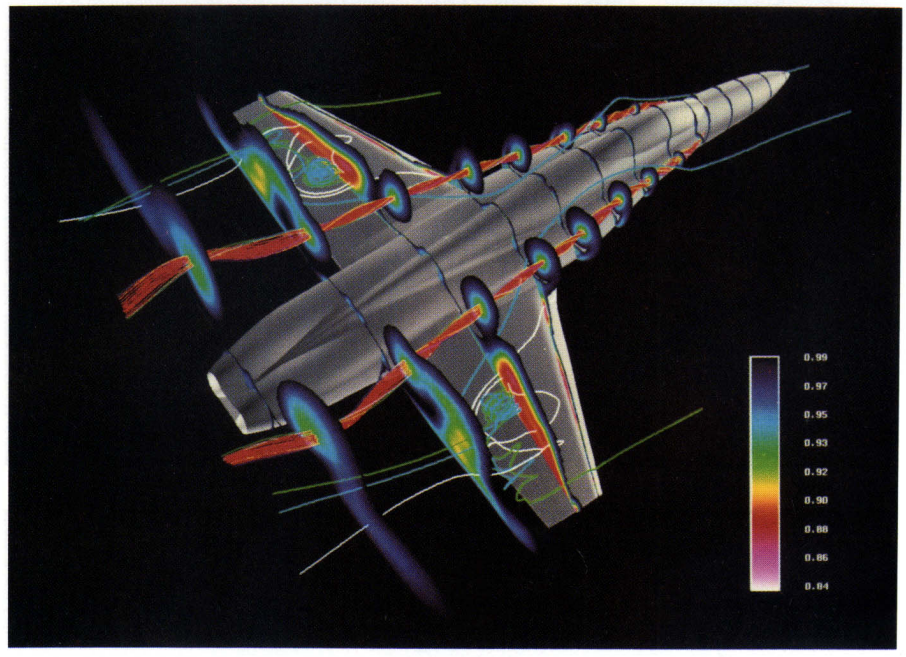

b) $\delta_f \approx 25$ deg

Fig. 6 Total pressure with streamline traces. $M_\infty = 0.34$, $R_c = 13.5 \times 10^6$, and $\alpha = 19$ deg.

viscous loss. The figure clearly reveals two major flow structures, one emanating from the LEX leading edge and the other developing over the wing. In general, the LEX primary and secondary vortex flow appear to be well-organized, up to the LEX wing leading-edge juncture, whereas the wing is experiencing stalled flow due to massive leading-edge flow separation. In an effort to visualize the chaotic flow behavior within the wing upper surface stagnant flow, the paths of three particles are shown, each distinguished with a different color (white, green, or cyan), released about the middle of the separated region and traced both upstream (computed with negative time) as well as downstream (computed with positive time). It is interesting to note that, for example, all three particles begin to loop around inside the wing separated-flow region before they actually leave the confinement. It appears that immediately aft of the LEX wing leading-edge juncture, the more energetic LEX vortical flow, no longer being fed from the LEX leading edge, starts to grow and lose its strength as it amalgamates with the more stagnant wing upper surface flow. This interaction results in a sudden core expansion of the LEX vortical flow which is evident in the last two crossflow planes. Note that the LEX and the wing flowfield are completely coalesced in the last plane. Furthermore, the total pressure contours shown over the wing indicate that the LEX-primary vortex sheet is being fed from the wing tip and encloses the entire wing flowfield, without developing any secondary flow structures. In addition, the figure shows several small flow structures such as the LEX-body juncture flow migrating downstream and also the canopy-body juncture flow just aft of the canopy, close to the plane-of-symmetry.

The results obtained for the F/A-18 configuration with the blended-flap setting are presented in Fig. 6b, over the same contour range and from the same vantage point as the previous figure. As expected, the flap deflection causes an increased circulation around the wing thereby energizing the stalled flow. This effect may be observed by contrasting the

size of the separated-flow region over the wing against the undeflected flap results of Fig. 6a. As a result, the LEX primary vortex flow does not appear to be influenced by the much smaller separated-flow region over the wing thus maintaining its tight core flow structure further downstream. In addition, the total pressure contours shown in the first crossflow plane over the wing, located slightly ahead of the flap hinge line, indicate only a small region of separated flow that is much flatter compared to the undeflected flap computations shown earlier in Fig. 6a. Also, in the same crossflow plane just outboard of the wing-fuselage juncture, note the development of a small isolated vortical flow that can be directly attributed to the negative dihedral introduced and confined to the blended flap region. Subsequently, this vortical flow appears to have been entrained by the larger separated wing flowfield. Particles are released at the same physical locations, with the same color assignments, in Figs. 6a and 6b. Similar to the results shown earlier for the undeflected flap computations, the released particles tend to wander around before piercing through the confined separated-flow region; see in particular the upstream tracings by blue and green streamlines. A more detailed discussion on the overall flow physics associated with the present computations can be found in Ref. 22.

The results presented in Fig. 6 indicate that the newly developed generalized surface patching algorithm produce excellent results for smooth interpolation of flow properties across various block boundaries. Furthermore, as discussed earlier, the undeflected flap result is used as a restart solution for the blended flap computation in order to accelerate the convergence. However, this approach may have hampered the normal convergence rate because the starting flow structure is massively separated, particularly over the wing surface.

An oblique top-view of the static surface pressure coefficients computed about the F/A-18 configuration with undeflected-flap is shown in Fig. 7a. The figure clearly depicts several flow characteristics such as the footprint of the low pressure associated with the LEX primary vortex system and the chaotic surface pressure pattern over the wing, indicative of a stalled flow. Note the disappearance of the LEX vortex

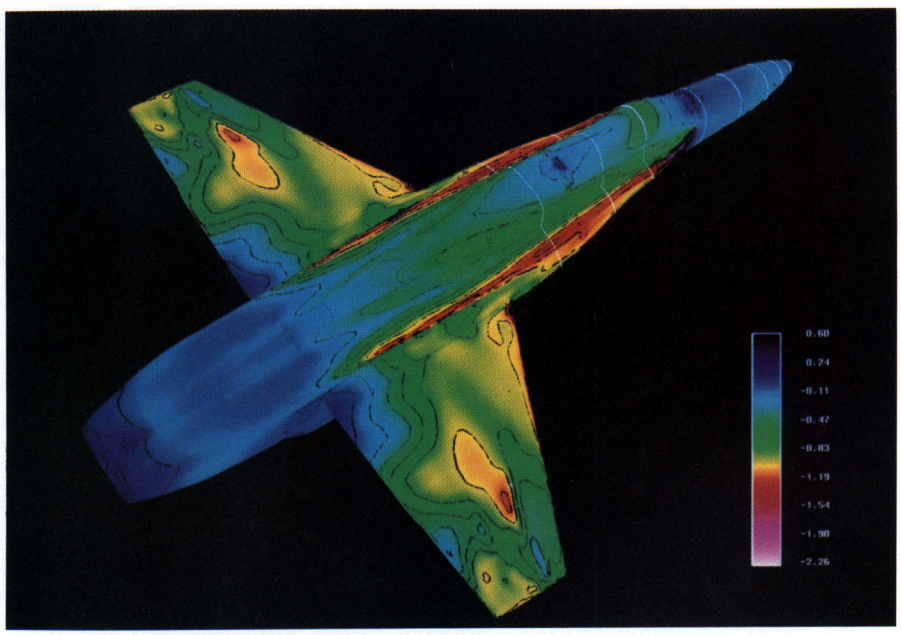

a) $\delta_f = 0$ deg

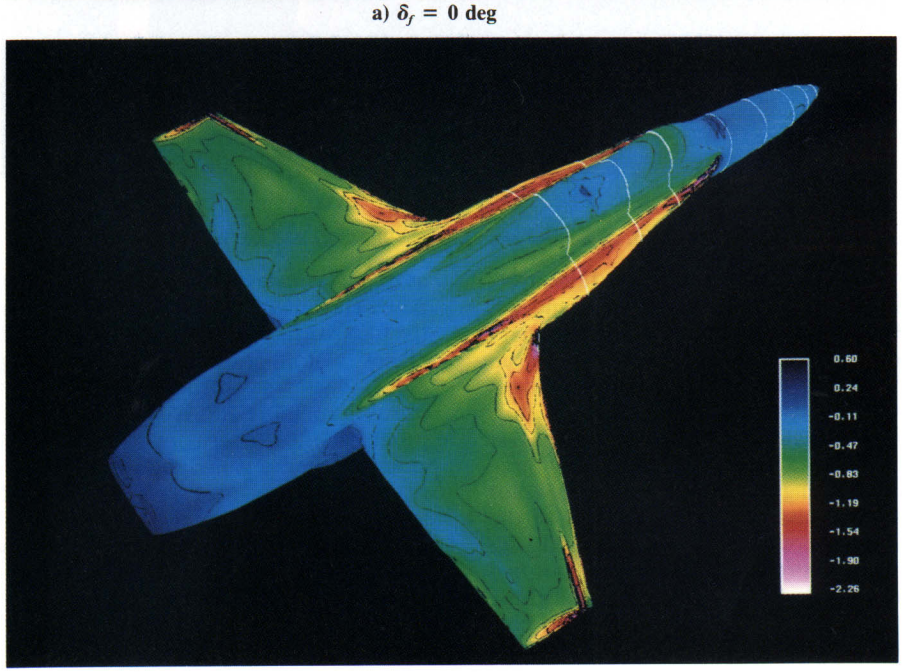

b) $\delta_f \approx 25$ deg

Fig. 7 Upper surface pressure coefficients. $M_\infty = 0.34$, $R_c = 13.5 \times 10^6$, and $\alpha = 19$ deg.

footprint on the fuselage near the wing trailing-edge/body juncture which can primarily be attributed to two factors. These factors include the loss of the strong LEX vortex feeding mechanism along with the radial movement of the vortex away from the surface as it passes longitudinally aft of the wing-LEX leading-edge juncture.

The same viewpoint is used to present the upper surface pressure coefficients computed for the blended flap configuration in Fig. 7b. In contrast to the undeflected flap results, this figure illustrates a much less chaotic pressure distribution over the wing surface. The figure shows a strong vortical flow developing over the wing apex that is mainly attributed to the blended flap region; this flow structure is also seen in Fig. 6b. Furthermore, there is evidence of a vortex-like separation at the flap hinge line over the outboard wing panel that subsequently merges with a small vortical tip flow. Although the surface pressures look very similar, particularly over the forebody and the LEX region, a more detailed assessment indicates some differences as will be discussed subsequently in conjunction with flight test data. Note that the stations at which the flight data have been measured are highlighted with white and are located at $x = 70$, 85, 107, 142, 184, 253, 296, and 357. All the body stations are given in full-scale inches and for reference the nose starts at $x \approx 60$.

Correlations with Flight Data

The computed surface pressure coefficients for both undeflected and the blended-flap configurations are presented in Fig. 8 at eight stations. The flight data[23] obtained at a slightly different flow conditions ($M_\infty = 0.30$, $R_{\bar{c}} = 11.5 \times 10^6$, and $\alpha = 19.1$ deg) are also shown for both the starboard as well as port sides to assess flow symmetry. The variation of the surface pressure coefficients as a function of azimuthal angle θ on the forebody are shown in Figs. 8a–e. The windward and the leeward sides of the forebody corresponds to $\theta = 0$ and 180 deg, respectively. In general, the upstream influence of the blended flap deflection is small and nearly constant on the forebody pressure distribution. At station 1, both results slightly underpredict the suction peak; however, the blended-flap solution correlates better with the data, par-

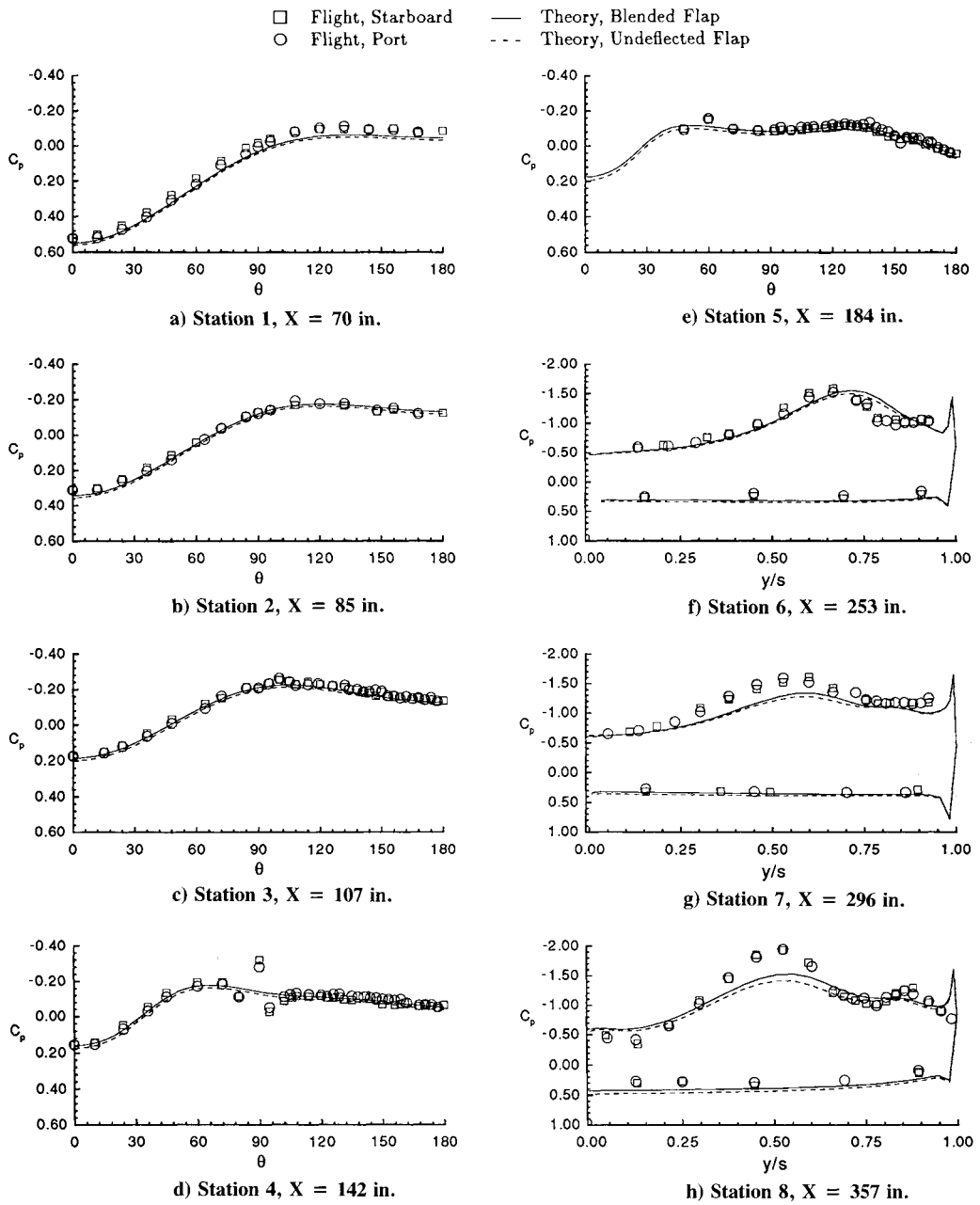

Fig. 8 Surface pressure correlations with flight data. (Theory: $M_\infty = 0.34$, $R_{\bar{c}} = 13.5 \times 10^6$, and $\alpha = 19$ deg; data: $M_\infty = 0.30$, $R_{\bar{c}} = 11.5 \times 10^6$, and $\alpha = 19.1$ deg.)

ticularly on the windward side. Note that this discrepancy could well be due to the expected transitional flow near the nose apex which is not modeled in the present computations. Furthermore, the disagreement at station 4 ($\theta \approx 90$ deg) is also attributed directly to an antenna fairing that exists on the HARV, but is not modeled here. Otherwise, the correlations between the flight data and theory, in particular the blended flap results, on the forebody are excellent.

The surface pressure coefficients computed on the LEX are shown in Figs. 8f–h along with the flight test results as a function of LEX exposed semispan y/s. In this way $y/s = 0$ corresponds to the LEX-body juncture and $y/s = 1$ corresponds to the LEX leading edge. Figure 8f shows a good correlation between the data and the theory, except in the outboard region which corresponds to the LEX secondary vortex flow. However, the correlation between the theory and data starts to deteriorate, particularly in terms of underpredicting the LEX vortex flow suction peak at station 7 (Fig. 8g), and continues to do so at station 8 (Fig. 8h). This degradation can be attributed to the lack of proper modeling of the gap region (i.e., closed/blended over in the present computations) between the inboard face of the deflected flap and the LEX as well as inlet propulsion simulation (closed/faired over). In particular, the proper modeling of the gap (i.e., flow through) is expected to strengthen the LEX vortical flow, due to the increased longitudinal length of the exposed LEX leading edge, and therefore, raise the neighboring vortical flow suction peak. Similar to the data/theory correlations discussed earlier on the forebody, Figs. 8f–h illustrate that the LEX surface pressures obtained from the blended flap computations also agree better with the data than the undeflected flap results.

The restricted surface flow pattern obtained on the F/A-18 configuration for both the undeflected flap (port) and blended flap (starboard) are shown in Fig. 9a from a nose-down front view perspective. The particle paths over the wing and fuse-

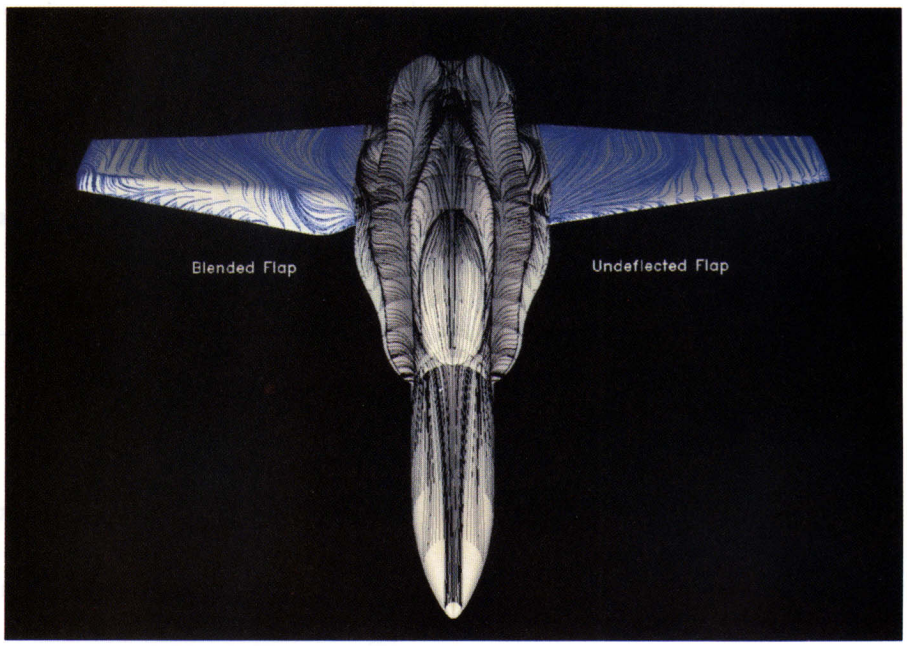

a) Computational result

b) In-flight result

Fig. 9 Restricted surface flow correlation. (Theory: $M_\infty = 0.34$, $R_c = 13.5 \times 10^6$, and $\alpha = 19$ deg; data: $M_\infty \approx 0.30$, $R_c \approx 10 \times 10^6$, and $\alpha \approx 20$ deg.)

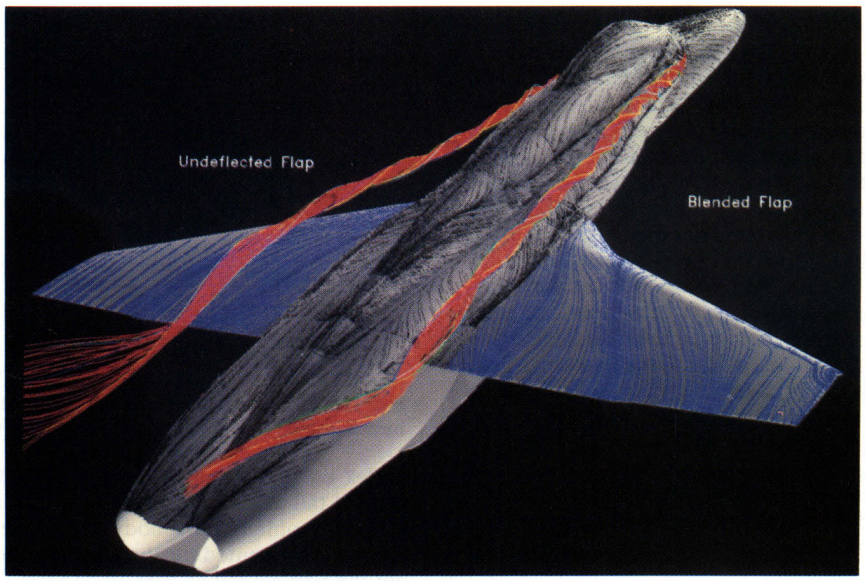

a) Computational result, restricted surface flow

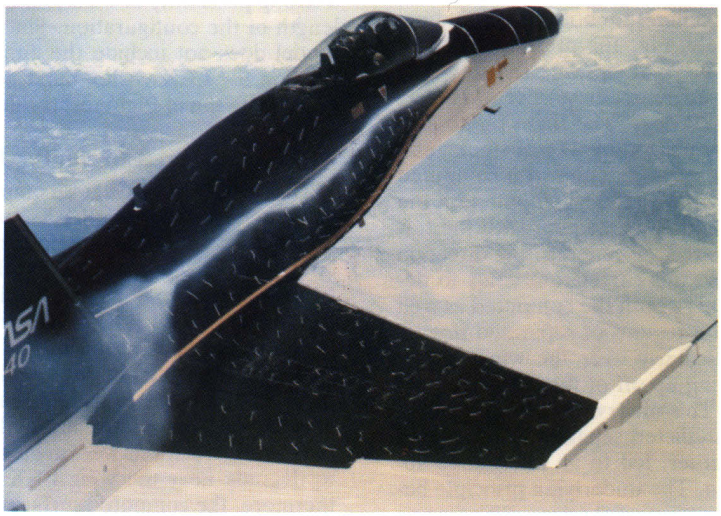

b) In-flight result

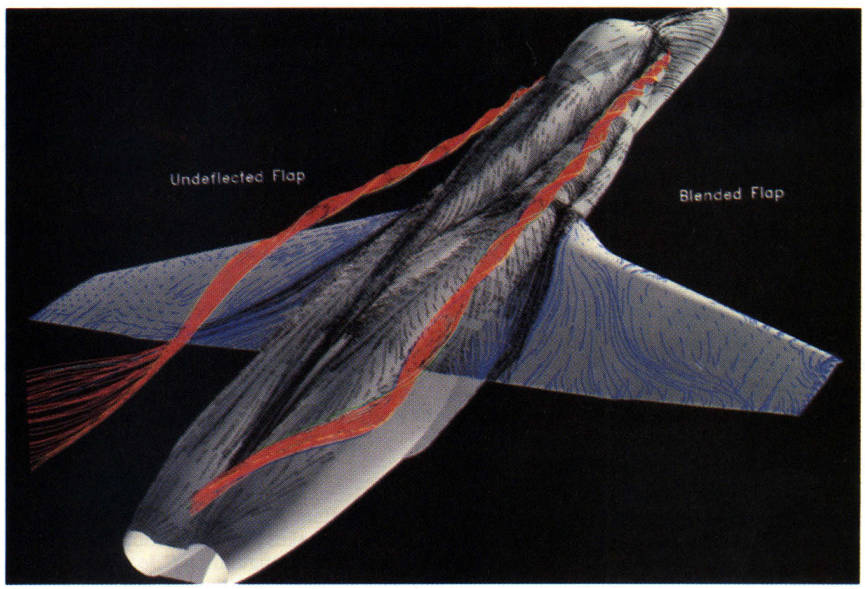

c) Computational result, unrestricted surface flow

Fig. 10 Surface/off-surface flow correlations with flight result. (Theory: $M_\infty = 0.34$, $R_{\bar{c}} = 13.5 \times 10^6$, and $\alpha = 19$ deg; data: $M_\infty \approx 0.30$, $R_{\bar{c}} \approx 10 \times 10^6$, and $\alpha \approx 20$ deg.)

lage-LEX configuration are highlighted with blue and black, respectively. The flow pattern over the forebody indicates a primarily attached flow structure for both undeflected as well as blended flap deflection with very little difference. Furthermore, the LEX surface flow pattern clearly illustrates the primary vortex reattachment line near the fuselage-LEX juncture along with a distinct secondary flow separation line and its corresponding reattachment line close to the leading edge. The wing leading-edge flap deflection does not appear to have a significant effect on the LEX surface flow pattern. However, as expected, the wing surface flow shows a drastic change, particularly around the leading edge. For example, the reattachment line that ran roughly parallel to the undeflected flap leading edge, now has moved aft, closer to the flap hinge line; also note the development of a separation line on the wing outboard panel right at the deflected flap hinge line. The forebody-LEX surface-flow pattern obtained in flight on the HARV is shown in Fig. 9b from a similar vantage point. The figure clearly reveals an excellent correlation between computed surface flow and the flight test results obtained, at the same flow conditions, on both the forebody as well as the LEX.

The same restricted surface flow pattern is shown in Fig. 10a, from a different vantage point, along with the corresponding LEX vortex core streamlines for both computational flap representations. Conversely, Fig. 10b presents a photograph of the HARV[21] taken in-flight showing the flow tuft survey over the wing and the LEX upper surface at ($M_\infty \approx 0.3$, $R_{\bar{c}} \approx 10 \times 10^6$, and $\alpha \approx 20$ deg). The flight photo also reveals the LEX vortex core visualized by way of smoke and will be discussed subsequently in conjunction with computed results. The restricted surface flow pattern computed on the fuselage and LEX are in qualitative agreement with the tuft survey observed in-flight, in terms of general flow direction and separation lines. However, this correlation tends to degrade over the wing surface where both the computed as well as the flight test results indicate regions of separated flow.

The flight tuft photo, particularly over the wing, shows individual tufts that are standing-up off of the surface as can be the case for a stalled flow. This observation, coupled with the prior knowledge of the predicted separated-flow region over the wing as discussed earlier, led to an alternative approach for tuft-flow simulation. The underlying principle behind this approach is to perform the particle streamline tracing without restricting the computations to any particular grid planes.

The above approach for tuft flow simulation was adopted to obtain the unrestricted surface flow pattern shown in Fig. 10c for both blended (starboard) and undeflected (port) flap configuration. As evident, this method produces a drastically different flow pattern, particularly over the wing where the flow is massively separated, which qualitatively resembles that observed in-flight (see Fig. 10b). Due to the stalled flow characteristics over the wing surface, the particle tracings (shown in Fig. 10c), are initiated at a plane slightly ($\approx$0.02 in. in full-scale dimension which is approximately $1.4 \times 10^{-4}\,\bar{c}$) off the surface where the flow velocity vectors become sufficiently large to produce a visible tuft flow pattern over a reasonable number of time steps. The new approach is clearly superior in simulating the separated tuft flows.

The flight photo (shown in Fig. 10b) clearly indicates that the LEX vortex burst is occurring just ahead of the vertical tail. It is also known that for generic fighter type aircraft experiencing vortical flow, the presence of the twin vertical tail induces pressure field that can precipitate vortex bursting. This effect has been shown experimentally[24] on the F/A-18 configuration. The experimental wind-tunnel study of Ref. 24 is conducted on a $\frac{1}{8}$th scale model of the F/A-18 aircraft at $M_\infty \approx 0.12$, $R_{\bar{c}} \approx 10^6$. The plot summarizing the effect of vertical tail presence on the LEX vortex burst position, at various angles of attack, is shown in Fig. 11 (courtesy of Ref. 24). The figure clearly indicates, for example, that the LEX

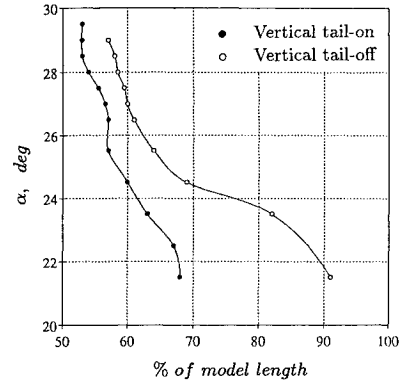

Fig. 11 LEX vortex burst position with/without vertical tail–wind-tunnel results. $M_\infty \approx 0.12$, $R_{\bar{c}} \approx 1 \times 10^6$ (Courtesy of Ref. 24).

vortex burst position, with and without the presence of the vertical tail at $\alpha = 21.5$ deg, occurs at about 68 and 91% of the total configuration body length, respectively. Although no data is presented for the LEX vortex burst position, without the vertical tail at $\alpha = 19$ deg (i.e., corresponding to the present computation), the trend of the reported data indicate a strong possibility of a burst-free LEX vortex over the entire length of the configuration. Since the present computational model does not include the empennage geometry, any correlation for LEX vortex burst position between the computations and the in-flight test results would rather be fortuitous.

Concluding Remarks

Thin-layer Navier-Stokes computations are presented about an accurate F/A-18 wing-LEX-fuselage configuration with both undeflected as well as the deflected leading-edge flap geometries. The results revealed that the wing with the undeflected flap is experiencing massive leading-edge flow separation indicative of stalled flow behavior. The leading-edge flap deflection significantly reduced the overall size of the separated flow over the wing but did not eliminate it. Excellent surface pressure correlations have been obtained on the forebody between the computational and flight-test results. Reasonable pressure correlations were achieved on the LEX which started to degrade near the wing LEX leading-edge juncture. Furthermore, the computed surface flow pattern obtained on the forebody and the LEX surface, which also included the presence of a seondary separation line, agreed qualitatively well with in-flight test results. A general computational approach has also been devised to simulate surface tuft-flow pattern that is particularly applicable to a massively separated-flow region. The results also indicated that the new generalized surface-patching method produced excellent results for smooth interpolation of flow properties across various blocks despite the complexity of the predicted flow.

Acknowledgments

NASA Langley Research Center sponsored the work of B. L. Bates and R. T. Biedron under NASA Contract NAS1-18585 and NAS1-19320, respectively. The authors wish to thank Dave Fisher of the NASA Dryden Flight Research Facility for providing the F/A-18 HARV flight test results and also Bruce Wedan of Vigyan Inc. for his assistance in generating the wing flowfield grid.

References

[1]Ghaffari, F., Luckring, J. M., Thomas, J. L., and Bates, B. L., "Navier-Stokes Solutions About the F/A-18 Forebody-Leading-Edge Extension Configuration," *Journal of Aircraft*, Vol. 27, No. 9, 1990, pp. 737–748.

[2]Thomas, J. L., Walters, R. W., Reu, T., Ghaffari, F., Weston, R. P., and Luckring, J. M., "Application of a Patched Grid Algorithm to the F/A-18 Forebody Leading-Edge Extension Configuration," *Journal of Aircraft*, Vol. 27, No. 9, 1990, pp. 749–756.

[3]Schiff, L. B., Cummings, R. M., Sorenson, R. L., and Rizk, Y. M., "Numerical Simulation of High-Incidence Flow over the F-18 Fuselage Forebody," AIAA Paper 89-0339, Jan. 1989.

[4]Benek, J. A., Steger, J. L., Dougherty, F. C., and Buning, P. G., "Chimera, A Grid Embedding Technique," ARDC-TR-85-64, Arnold AFS, TN, 1986.

[5]Buning, P. G., Chiu, I. T., Obayashi, S., Rizk, Y. M., and Steger, J. L., "Numerical Simulation of the Integrated Space Shuttle Vehicle in Ascent," AIAA Paper 88-4359, Aug. 1988.

[6]Cummings, R. M., Rizk, Y. M., Schiff, L. B., and Chaderjian, N. M., "Navier-Stokes Predictions of the Flowfield Around the F-18 (HARV) Wing and Fuselage at Large Incidence," AIAA Paper 90-0099, Jan. 1990.

[7]Rizk, Y. M., Schiff, L. B., and Gee, K., "Numerical Simulation of the Viscous Flow Around a Simplified F/A-18 at High Angles of Attack," AIAA Paper 90-2999, Aug. 1990.

[8]Rizk, Y. M., and Gee, K., "Numerical Prediction of the Unsteady Flowfield Around the F-18 Aircraft at Large Incidence," AIAA Paper 91-0020, Jan. 1991.

[9]Biedron, R. T., and Thomas, J. L., "A Generalized Patched-Grid Algorithm with Application to the F-18 Forebody with Actuated Control Strake," *Computing Systems in Engineering*, Vol. 1, Nos. 2–4, 1990, pp. 563–576.

[10]Thomas, J. L., and Newsome, R. W., "Navier-Stokes Computations of Lee-Side Flows over Delta Wings," *AIAA Journal*, Vol. 27, No. 12, 1989, pp. 1673–1679.

[11]Thomas, J. L., Taylor, S. L., and Anderson, W. K., "Navier-Stokes Computations of Vortical Flows over Low Aspect Ratio Wings," *AIAA Journal*, Vol. 28, No. 2, 1990, pp. 205–212.

[12]Vatsa, V. N., Thomas J. L., and Wedan, B. W., "Navier-Stokes Computations of a Prolate Spheroid at Angle of Attack," *Journal of Aircraft*, Vol. 26, No. 11, 1989, pp. 986–993.

[13]Ghaffari, F., Luckring, J. M., Thomas, J. L., and Bates, B. L., "Navier-Stokes Solutions About the F/A-18 Forebody-LEX Configuration," AIAA Paper 89-0338, Jan. 1989.

[14]Baldwin, B. S., and Lomax, H., "Thin Layer Approximation and Algebraic Model for Separated Turbulent Flows," AIAA Paper 78-257, Jan. 1978.

[15]Degani, D. and Schiff, L. B., "Computation of Supersonic Viscous Flows Around Pointed Bodies at Large Incidence," AIAA Paper 83-0034, Jan. 1983.

[16]Roe, P. L., "Characteristic Based Schemes for the Euler Equations," *Annual Review of Fluid Mechanics*, Vol. 18, 1986, pp. 337–365.

[17]Van Leer, B., "Upwind-Difference Method for Aerodynamic Problems Governed by the Euler Equations," *Lectures in Applied Mathematics*, Vol. 22, 1985, pp. 327–336.

[18]Smith, B. M., Brauner, K. M., Kennicott, P. R., Liewald, M., and Wellington, J., "Initial Graphics Exchange Specification (IGES)," Version 2.0, U.S. Dept. of Commerce, Rept. NBSIR 82-2631 (AF), Feb. 1983.

[19]Brewer, J. A., and Anderson, D. C., "Visual Interaction with Overhauser Curves and Surfaces," *Proceedings of the 4th Annual Conference on Computer Graphics and Interactive Techniques*, American Society of Mechanical Engineers, San Jose, CA, July 20–22, 1977, pp. 132–137.

[20]Ghaffari, F., Luckring, J. M., Thomas, J. L., and Bates, B. L., "Transonic Navier-Stokes Solutions About a Generic Hypersonic Configuration," *Journal of Aircraft*, Vol. 28, No. 6, 1991, pp. 381–388.

[21]Fisher, D. F., Del Frate, J. H., and Richwine, D. M., "In-Flight Visualization Characteristics of the NASA F-18 High Alpha Research Vehicle at High Angles of Attack," NASA-TM 4193, May 1990.

[22]Ghaffari, F., Bates, B. L., Luckring, J. M., Thomas, J. L., and Biedron, R. T., "Navier-Stokes Solutions About the F/A-18 Wing-LEX-Fuselage Configuration with Multi-Block Structured Grids," AIAA Paper 91-3291, Sept. 1991.

[23]Fisher, D. F., NASA Dryden Flight Research Facility.

[24]Martin, C. A., and Thompson, D. H., "Scale Model Measurements of Fin Buffet Due to Vortex Bursting on F/A-18," 68th Fluid Dynamics Panel Specialists Meeting on Maneuvering Aerodynamics, AGARD Paper 12, Toulouse, France, May 1–2, 1991.